J_ID: APRPG5 DOI: 10.1063/5.0040732 Date: 17-March-21 Stage: Page: 1 Total Pages: 15

PROOF COPY [APR20-AR-01054]

Applied Physics Reviews ARTICLE scitation.org/journal/are

Controlling cellular organization in bioprinting through designed 3D microcompartmentalization

Cite as: Appl. Phys. Rev. 8, 000000 (2021); doi: 10.1063/5.0040732
Submitted: 15 December 2020 · Accepted: 9 March 2021 ·
Published Online: 0 Month 0000

View Online Export Citation CrossMark

Mohamadmahdi Samandari,[1,2] Fatemeh Alipanah,[3] Keivan Majidzadeh-A,[2] Mario M. Alvarez,[4] Grissel Trujillo-de Santiago,[4,5] and Ali Tamayol[1,a)]

AFFILIATIONS

[1]Department of Biomedical Engineering, University of Connecticut Health Center, Farmington, Connecticut 06030, USA
[2]Breast Cancer Research Center, Motamed Cancer Institute, ACECR, P.O. Box 15179/64311, Tehran, Iran
[3]Applied Physiology Research Center, Department of Physiology, Cardiovascular Research Institute, Isfahan University of Medical Sciences, Isfahan 81746-73461, Iran
[4]Centro de Biotecnología-FEMSA, Tecnologico de Monterrey, Monterrey, Nuevo León 64849, Mexico
[5]Departamento de Mecatrónica y Eléctrica, Tecnologico de Monterrey, Monterrey, Nuevo León 64849, Mexico

[a)]Author to whom correspondence should be addressed: atamayol@unl.edu

ABSTRACT

Controlling cellular organization is crucial in the biofabrication of tissue-engineered scaffolds, as it affects cell behavior as well as the functionality of mature tissue. Thus far, incorporation of physiochemical cues with cell-size resolution in three-dimensional (3D) scaffolds has proven to be a challenging strategy to direct the desired cellular organization. In this work, a rapid, simple, and cost-effective approach is developed for continuous printing of multicompartmental hydrogel fibers with intrinsic 3D microfilaments to control cellular orientation. A static mixer integrated into a coaxial microfluidic device is utilized to print alginate/gelatin-methacryloyl (GelMA) hydrogel fibers with patterned internal microtopographies. In the engineered microstructure, GelMA compartments provide a cell-favorable environment, while alginate compartments offer morphological and mechanical cues that direct the cellular orientation. It is demonstrated that the organization of the microtopographies, and consequently the cellular alignment, can be tailored by controlling flow parameters in the printing process. Despite the large diameter of the fibers, the precisely tuned internal microtopographies induce excellent cell spreading and alignment, which facilitate rapid cell proliferation and differentiation toward mature biofabricated constructs. This strategy can advance the engineering of functional tissues.

I. INTRODUCTION

Cells in most tissues exhibit a high level of organization in their spatial distribution and alignment.[1,2] This organized architecture is critical to proper cellular development during maturation and the function of the mature tissue. Therefore, biofabricated cellular scaffolds for tissue engineering applications need to mimic this cellular architecture to reproduce the behaviors of natural tissue.[3,4] Various chemical or topological surface patterning approaches have been employed to provide cues for controlling the alignment of the cells, but these methods are limited to 2D culture and fail to translate into realistic *in vivo* conditions.[5–7] Researchers also have endeavored to fabricate 3D scaffolds with controlled spatial distribution and directed alignment of the cells for various tissue engineering applications.[8,9] Cellular alignment in 3D scaffolds can be directed with similar chemical and topological patterning approaches to those currently used in 2D cell alignment. In some examples of such a technique, researchers used focused laser beams to pattern bioactive molecules inside 3D hydrogel scaffolds, which induced cellular elongation in a desired direction.[10,11] Furthermore, it has been demonstrated that confinement of cells in constructs with sufficiently small dimensions, fabricated through micromolding or photolithography, can direct elongation of the cells along the borders of the structure.[12–14] Modulation of cellular alignment is also shown to be possible through application of external stimuli, such as static and dynamic mechanical

ID: aipepub3b2server Time: 21:58 I Path: D:/AIP/Support/XML_Signal_Tmp/AI-ARE#210028

J_ID: APRPG5 DOI: 10.1063/5.0040732 Date: 17-March-21 Stage: Page: 2 Total Pages: 15
PROOF COPY [APR20-AR-01054]

stress[15,16] or electrical pulses.[17,18] While these methods have been shown to successfully fabricate miniaturized tissue models, they suffer from significant limitations, such as setup complexity, the negative impact of external fields on cells, limited construct size, multistep fabrication processes, and low throughput, presenting significant challenges for their clinical translation.

Re-creating a highly organized hierarchical structure is of particular importance when engineering anisotropic fibrillar tissues, such as muscles.[19,20] The directionality in these structures spans from their microscale cellular alignment to the macroscale, where densely packed fibers bundle together to form fascicles.[21,22] As a result, microengineered cellular structures need to be assembled using relevant strategies that enable this organization. Fiber-based biofabrication techniques have been implemented for engineering anisotropic tissues, such as muscles, due to the similarity of the formed fibrillar architectures and the native tissue.[23,24] Ranging from extrusion bioprinting[25–27] to biotextile processes,[28] fiber-based tissue engineering has been employed as a high-throughput, simple, and cost-effective method for assembly of cell-laden fibers. These fibers act as the building blocks of biomimetic fibrillar constructs for engineering muscle. Inherent directionality, enhanced mechanical properties, and control over geometry and composition of final structure are distinct advantages of fiber-based approaches in the context of muscle tissue engineering.[23,24] However, creating highly ordered cellular organization within the individual fibers of such constructs has proven challenging, since the dimensions of fibers compatible with biotextile processes and extrusion bioprinting are much larger than cell-scale sizes, reducing the boundary effects on cellular organization.[20,29] It has been demonstrated that the encapsulated cells' alignment decreases with increasing distance between the boundaries, with microfeatures larger than 100 μm being unrecognizable to cells.[12]

A few approaches were successful in directing cellular organization in fiber-based scaffolds by incorporating intrinsic microstructures that provided guiding cues to the cells during their growth.[30,31] However, these methods require multistep fabrication processes, which makes them incompatible with bioprinting strategies. Here, we address this challenge by creating a compartmentalized fiber with internal hydrogel-based topographical cues to direct cellular growth and organization during tissue maturation. While controlling the fiber diameter in larger scales, the size of each compartment could also be easily tuned down to dimensions recognizable by cells to allow effective direction of cellular alignment within the fiber. To demonstrate the potential of the strategy, we investigated the effect of this biofabricated architecture on muscle cell growth, morphology, and function. This strategy can be easily applied to various fiber-based tissue engineering approaches, including 3D bioprinting and biotextile manufacturing, to control cellular organization, facilitating biofabrication of more biomimetic structures.

II. RESULTS

The process of fabricating multicompartmental hydrogel fibers (MCHFs) is depicted in Fig. 1. The proposed approach is based on the manipulation of different hydrogels' flow for construction of a compartmentalized stream of the bioink. Alginate and GelMA were selected as hydrogels for this purpose. One of the main challenges in fiber-based biofabrication approaches, such as extrusion bioprinting and biotextile manufacturing, is the selection of a "cell-favorable" bioink that can form a scaffold with high shape fidelity. This requires a relatively viscous precursor that can rapidly cross-link upon printing to form a robust and stable fiber.[28,32]

GelMA is a cell-permissive hydrogel that supports cell spreading and proliferation due to the presence of cell attachment sites, such as arginine-glycine-aspartic acid peptides, as well as matrix metalloproteinase–sensitive degradation motifs, suitable for cell remodeling.[33,34] However, due to its low viscosity and noninstantaneous photocrosslinking, direct formation of stable GelMA fibers is challenging.[35] A possible solution to overcome this is the incorporation of other hydrogels to enable GelMA fiber formation.[35] Alginate is a good candidate for mixing because it exhibits the necessary viscosity and rapid ionic gelation.[36] A hybrid GelMA/alginate bioink can easily be implemented in bioprinting[37] or biotextile strategies,[29] although the incorporation of alginate, which lacks cell attachment sites and biodegradable peptides, reduces the suitability of such bioinks for tissue engineering applications.[38]

In this study, we resolve this challenge through compartmentalization of the bioinks in such a way that distinct GelMA compartments support cell functionality while alginate compartments enable quick formation of stable fibers. A static mixer–integrated coaxial microfluidic device was employed for fabrication of MCHFs [Fig. 1(a) and Fig. S1]. A static mixer with an optimized number of mixing elements was implemented to divide the main streams of alginate and GelMA solutions into substreams with the desired thickness. This solution, with intercalated striations of GelMA and alginate, was then extruded through the inner channel of a coaxial microfluidic device and exposed to Ca^{2+} ions to stabilize the structure through gelation of the alginate. At this stage, the cross-linked alginate was physically confining the striations of GelMA precursor [Fig. 1(a), (i)]. UV irradiation was subsequently used to cross-link the GelMA within the alginate matrix and form internal microfilaments [Fig. 1(a), (ii)]. The final structure was a millimeter-scale hydrogel fiber with microscale internal topological features consisting of consecutive microfilaments of alginate and GelMA hydrogel. This multiscale fibrous structure can enable cells' spreading and alignment.

The subdivision of the different hydrogel streams into microscale substreams, embedded within the millimeter-scale flow, led to formation of internal features of a much smaller size than the diameter of the printed filament [Fig. 1(b)]. In conventional bioprinters, the minimum feature size in dictated by the nozzle diameter. As a result, improving the resolution comes at the cost of an increase in the shear stress applied to the encapsulated cells as well as an elevated pressure required for extrusion of viscous bioinks through the smaller nozzle.[39] However, in our printing strategy, resolutions are not shear dependent and are improved through the consecutive subdivision of streams without changing the nozzle diameter [Fig. 1(b), (i)]. Numerical simulation results demonstrated that while increasing the resolution using the static mixer does not significantly increase the shear stress inside the flow, a corresponding decrease in nozzle tip diameter to match the resolution enhanced with each additional static mixer element can increase the shear stress by approximately eightfold [Fig. 1(b), (ii) and (iii)]. Similarly, the extrusion pressure is not significantly increased by the static mixer due to its relatively large channel size (~5 mm; see Fig. S1), while the pressure increased by ~15-fold with decreasing the size of nozzle tip corresponding to the application of each additional static mixer element.

ID: aipepub3b2server Time: 21:58 I Path: D:/AIP/Support/XML_Signal_Tmp/AI-ARE#210028

J_ID: APRPG5 DOI: 10.1063/5.0040732 Date: 17-March-21 Stage: Page: 3 Total Pages: 15

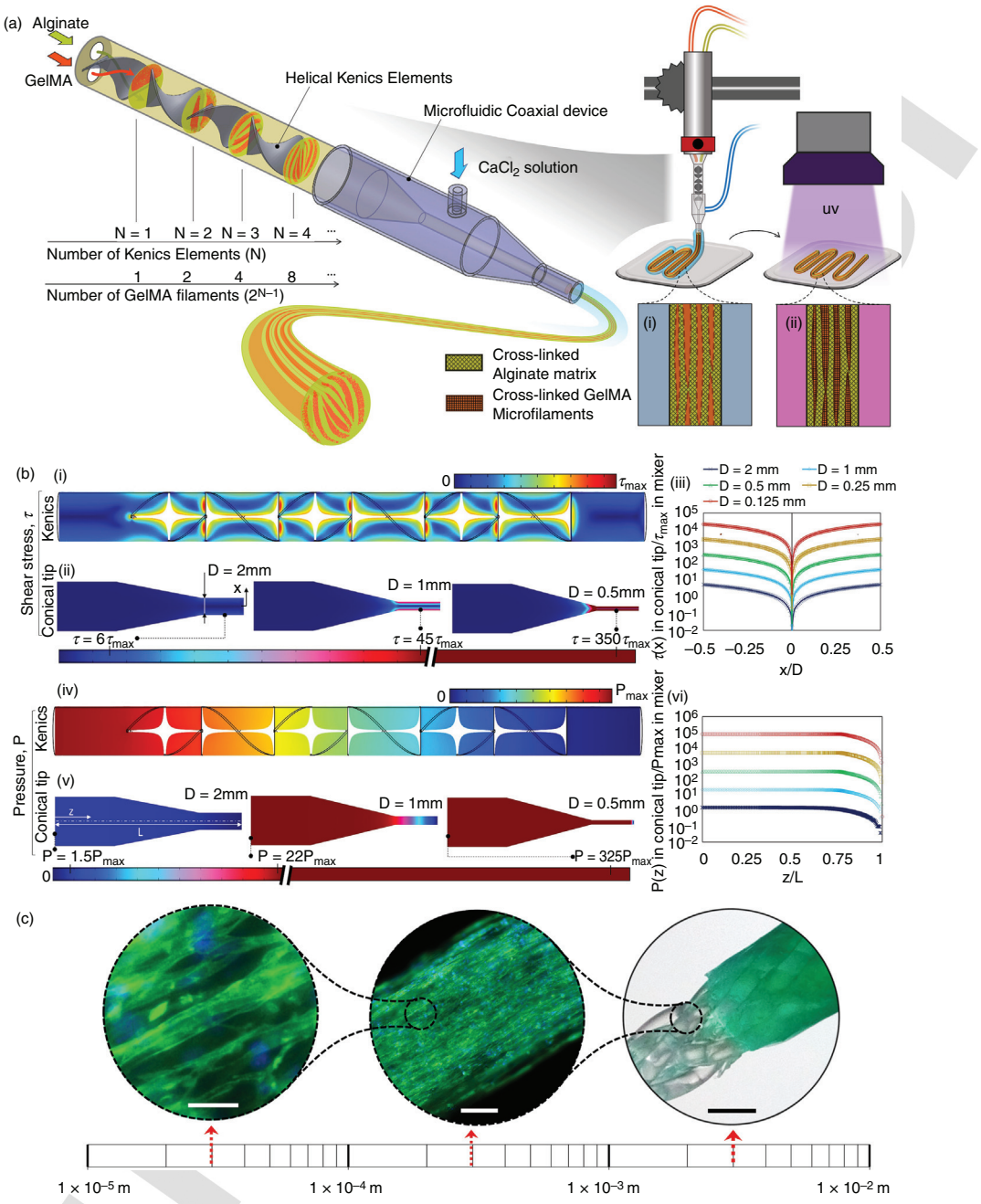

FIG. 1. Biofabrication of multicompartmental hydrogel fibers for formation of multiscale biomimetic constructs. (a) The fabrication setup consisted of a static mixer creating striations of different hydrogels integrated with a coaxial microfluidic device extruding the mixed streams of hydrogels through a sheath flow of $CaCl_2$ to cross-link alginate and form the matrix of the fiber (i). The fibers were then exposed to UV light to cross-link the GelMA striations within the alginate matrix, creating an internal fibrous microstructure (ii).

AQ14

Alignment of cells within the hydrogel fiber, as will be discussed in Secs. II A–D, could establish a hierarchical multiscale construct, mimicking the structure of native fibrillar tissue [Fig. 1(c)]. The fabrication method developed here is simple and cost effective, without any requirement for special tools. In addition, its high throughput allows the fabrication of cell-laden fibers at speeds up to meters per minute and makes this method attractive for unconventional applications of tissue engineering that requires mass production, such as lab-grown meat.

AQ2

J_ID: APRPG5 DOI: 10.1063/5.0040732 Date: 17-March-21 Stage: Page: 4 Total Pages: 15

A. Characterization of multicompartmental hydrogel fibers

The formation of MCHFs with internal microfilaments is based on the controlled mixing of the two constituent precursors in the mixing nozzle (Fig. 2). A computational finite element simulation was implemented to elucidate the working principle of the static mixer–integrated coaxial microfluidic device. Figure 2(a) shows the computer-aided design (CAD) model of the static mixer used for the simulations. In this study, a Kenics-type static mixer,[40,41] which consists of multiple helical elements twisting intermittently in different directions, was used for formation of MCHFs [Fig. 2(a)]. As indicated by simulations, each Kenics element in this setup divides the upstream of the flow into two substreams [Fig. 2(b)]. By injecting two different solutions into the mixer, the streams are consecutively divided into more substreams, forming an array of different striations. The total number of striations created using an N-element static mixer is therefore 2^N, while the number of striations for each component will be 2^{N-1}. Assuming a uniform distribution, the thickness of each striation is then $D_f/2^N$, where D_f is the final fiber diameter. Consequently, by controlling the number of elements in the static mixer, an internal structure with tunable thickness and number of striations can be formed. The cross section of flow clearly demonstrates the formed striations within the flow [Fig. 2(c), top row].

The simulation results were validated experimentally. The Kenics element CAD design was 3D printed using a stereolithography 3D printer followed by its insertion into a barrel and integration with a coaxial microfluidic device [Fig. S1(a)]. The device was then used for evaluation of the flow profile generated by the static mixer. Immediate cross-linking of the structure through wet spinning of alginate into a calcium chloride ($CaCl_2$) bath can preserve the internal microstructure of the fabricated fibers for analysis. Examining cross sections of experimentally generated fibers confirmed the formation of striations within the flow, which were cross-linked and formed the internal microfilaments. Figure 2(c), bottom row, indicates the size dependency of the microfilaments to the number of the mixer elements.

Multicompartmental alginate/GelMA fibers were fabricated using the two-step cross-linking process just described. Figure 2(d) indicates the effect of mixing level on the internal microstructure of the fibers fabricated using this method. As expected, a fibrous structure can be generated in which increasing the number of Kenics elements decreases the size of internal microfilaments [Fig. 2(d), (i) and (ii)]. Comparatively, a premixed bioink, prepared via vortex mixing and extruded through a static mixer–integrated microfluidic coaxial device, formed a homogeneous fiber without internal microfilaments [Fig. 2(d), (iii)].

To demonstrate that the developed multicompartmental printing is not limited to the implemented materials (alginate and GelMA) or their specific cross-linking methods, we evaluated the compatibility of the strategy with two different materials, including Pluronic-F127 and Laponite nanoclay hydrogels. Our results demonstrated that the internal microfilaments could be easily formed and preserved upon printing. Figure S2 illustrates the cross section and top view of the nanoclay MCHFs.

We further investigated the effect of the coaxial microfluidic device on the hydrogel fiber structure. The primary role of the coaxial microchannels is the induction of alginate gelation, making the fabrication strategy compatible with extrusion-based bioprinting. The coaxial system further provides the opportunity of accurate control over the diameter of fabricated hydrogel fibers [Figs. 2(e) and 2(f)]. Although the diameter of the fabricated fiber can also be adjusted by changing the size of the nozzle outlet, tuning the ratio of outer ($CaCl_2$ solution) channel flow rate Q_{out} to that of inner (multicompartmental hydrogel solution) channel Q_{in} offers real-time and accurate control over the size of final fiber. Simulation and experimental results demonstrated that by adjusting the Q_{out}/Q_{in} ratio, the orientation of internal microfilaments can be manipulated [Figs. 2(f) and 2(g)]. While a ratio of $Q_{out}/Q_{in} \approx 1$–2 did not significantly change the orientation of formed internal microfilaments, a higher ratio could deform the streamlines, as shown by simulation results. Immediate gelation of alginate upon exposure to Ca^{2+} ions could preserve the formed microstructure and even intensify it by solidifying the outer layers of the fiber while the fluid is still flowing in the inner layers.

The capability to independently tune both the size of the final fiber and its internal microfilaments provides the opportunity to implement current extrusion-based bioprinters while improving resolution down to cell-size scales. This multiscale biofabrication strategy specifically offers the formation of fibrous tissues with any target size while maintaining the capacity of the scaffold to direct cellular organization. The multicompartmental microstructure further provides the opportunity to harness the advantages of different biomaterials.

B. Directing cellular organization with multicompartmental hydrogel fibers

The multicompartmental fiber biofabrication strategy enabled directing cellular organization. Cells were encapsulated in GelMA precursor, and MCHFs were fabricated as previously described. Figure 3 compares the behavior of myoblasts cultured within the MCHFs with those cultured in fibers fabricated with premixed bioink. Despite the large (>1 mm) diameter of the fibers compared with the cell size, a highly aligned cellular organization was observed in MCHFs 24 h postfabrication [Fig. 3(a)], while the cells encapsulated in premixed fibers remained almost spherical [Fig. 3(b)]. The cellular alignment within the multicompartmental hydrogel fibers can be explained by (i) differential favorability of the cells for spreading in GelMA microfilaments over the alginate sections, (ii) fibrous internal microstructure acting as topological cues for directing cellular alignment, and (iii) mechanical stimulation of the cells due to differential mapping of scaffold stiffness in GelMA and alginate sections.

Since alginate does not have bioactive sequences, it acts as a cell-repellant compartment in the fiber structure, and therefore induces cell spreading inside internal GelMA microfilaments. Furthermore, the presence of 3D microtopographies of comparable size to the cell dimensions can direct cellular alignment along the microcompartment interfaces. As described previously, for a fiber with a diameter of ~1 mm, a static mixer with five to six Kenics elements forms internal GelMA microfilaments with an average size of 15–30 μm. Our data suggest that a higher level of mixing leads to formation of fibers without distinct regions due to miscibility of aqueous GelMA and alginate precursors. Upon exposure to Ca^{2+} ions, alginate immediately cross-links, which is accompanied by structure shrinkage,[42] squeezing out the liquid GelMA from the construct before photocrosslinking (Fig. S3). A decreased level of mixing, which consequently reduces the entrapment of the GelMA striations, therefore causes leaching of large portions of GelMA, leaving behind only non–cell-permissive alginate.

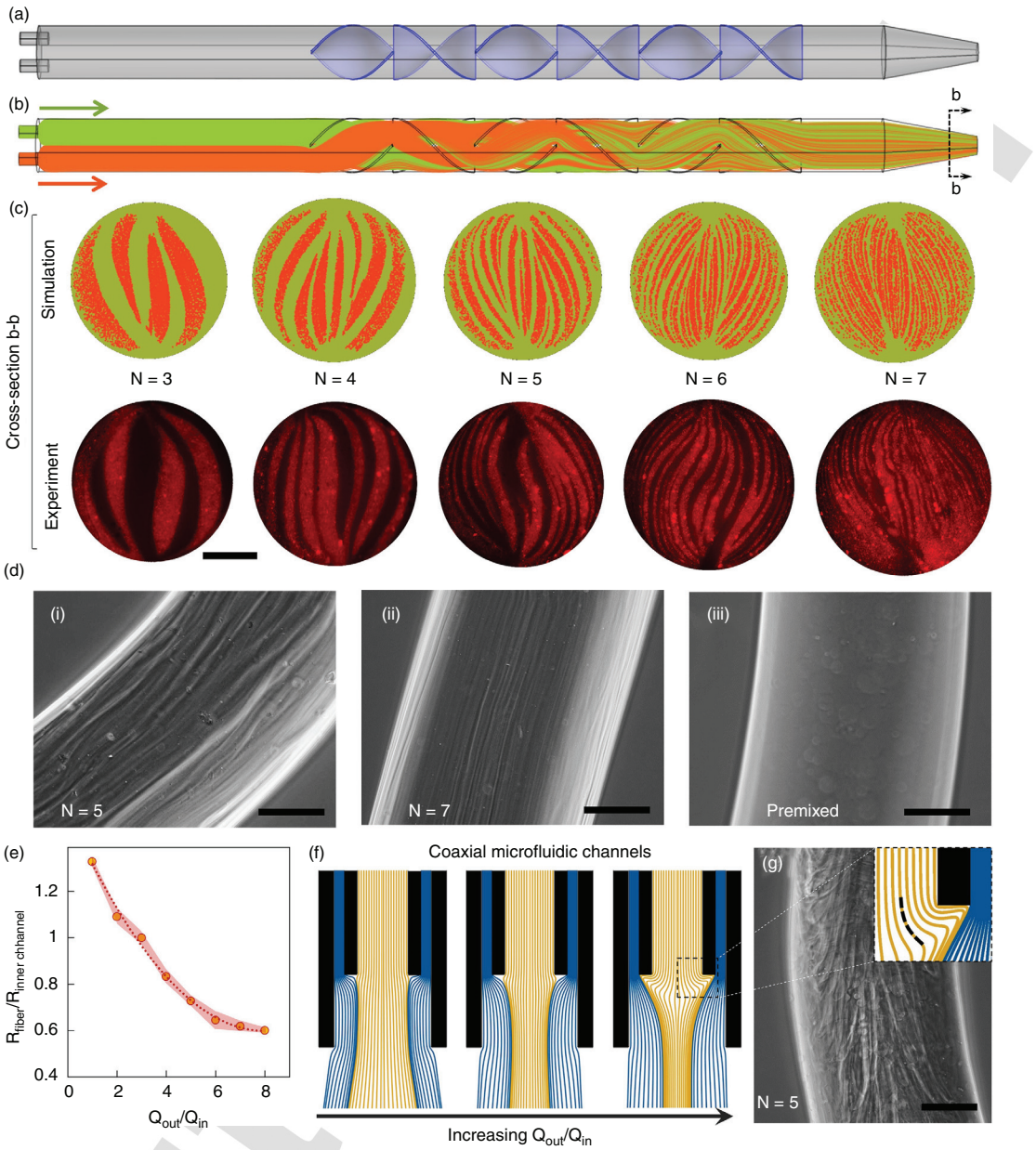

FIG. 2. Characterization of multicompartmental hydrogel fibers. (a) Representative design of Kenics static mixer with helical elements used for flow characterization via finite element simulations. (b) The working principle of the Kenics static mixer is demonstrated using simulation results. Two streams of hydrogel precursors were introduced at the inlets of the static mixer and then consecutively divided into substreams by Kenics elements followed by their blending as a result of helical profile of the elements. (c) A cross section of the multicompartmental stream (top row, simulation results) or fabricated hydrogel fiber (bottom row, experimental results) demonstrating the effect of number of elements on the number and size of internal microstructure. N stands for the number of consecutive elements in the mixer. Scale bar is 500 μm. (d) Phase contrast images of multicompartmental alginate/GelMA fibers demonstrating the fiber's internal microfilaments. Increasing the number of mixing elements decreased the size of the microfilaments. Subpanels (i) and (ii) correspond to the fibers fabricated using the Kenics static mixer with five and seven elements, respectively, while subpanel (iii) shows the fabricated fiber with a premixed bioink prepared through vortex mixing and heating at 80 °C. Scale bars are 200 μm. (e) The control over the fiber diameter using the coaxial microfluidic device. While the diameter of the fiber can be manipulated by changing the diameter of the internal channel in the coaxial device, it can also be tuned finely by adjusting the inner and outer channel flow rates (Q_{in} and Q_{out}, respectively). R_{fiber} and R_{inner} channel indicate the radius of the fabricated hydrogel fiber and the radius of the inner channel in the coaxial microfluidic device, respectively. n = 3 for each measurement point. (f) The simulation results demonstrating the effect of Q_{out}/Q_{in} ratio on the diameter of the fabricated fiber. Blue streamlines show the flow of $CaCl_2$, and yellow streamlines represent the hydrogel mixture flow (Q_{out}/Q_{in} = 1, 3, and 8, respectively, from left to right). (g) The effect of flow rates on organization of internal microfilaments. Increasing the Q_{out}/Q_{in} ratio deforms the streamlines of the hydrogel mixture and therefore changes the orientation of the internal microfilaments. Scale bar is 200 μm.

The difference in mechanical properties of alginate and GelMA hydrogels can further induce cellular alignment as a result of mechanical stimulation. Figure S4 demonstrates the significant difference between mechanical properties of the alginate and GelMA hydrogels used in this study. It has been shown that the presence of stiff geometrical constraints (anchoring sites), which can restrict the movement of cell-containing hydrogels, induce cellular alignment and maturation, specifically in contractile tissues.[43] The cellular alignment in these systems arises from mechanical stimulation generated by a cytoskeleton-mediated internal tension along the lines passing between the hydrogel anchoring sites.[15,44] Many studies have reported the application of stiff geometrical constraints for anchoring the cell-laden hydrogel and therefore inducing cellular alignment.[27,45] Specifically, it has been demonstrated that an alignment in the geometry of stiff anchoring sites can align cells more effectively.[43,44] In our system, aligned alginate microfilaments with significantly higher elastic modulus compared to GelMA can act as anchoring sites, constraining the cell-laden GelMA hydrogel, and therefore induce alignment. The application of alginate as a stiff hydrogel within soft hydrogel networks has been previously reported for controlling cellular shape and spreading.[46]

A quantitative evaluation of cell orientation in the multicompartmental hydrogel fibers demonstrated an almost uniaxial organization of both cytoskeleton and nuclei along the fiber axis [Fig. 3(c)]. The alignment of the nuclei is of specific importance due to the crucial role of nuclei morphology in cellular behavior, affecting their metabolic activity, protein expression, and differentiation.[3] We further demonstrated that the multicompartmental hydrogel fibers support cellular proliferation, in contrast to the fibers fabricated from the premixed bioink [Fig. 3(d)]. The presence of distinct GelMA regions in the engineered construct ensures cell spreading and proliferation. However, in the premixed structure, the presence of alginate does not allow scaffold degradation and therefore does not offer enough space for proper cell spreading and proliferation. As a result, the activity of the cells, and therefore their rate of proliferation, decreased over time. Due to the limited biocompatibility of the hydrogel fibers fabricated with premix bioink, specifically in longer-term studies, we excluded them from the future experiments.

We demonstrated the potential of the proposed biofabrication strategy for directing alignment of the cells along the fiber axis, while supporting cellular activity and function. Since cells follow the fiber direction (Fig. S5), their orientation inside the scaffold can be easily controlled by adjusting the orientation of the fiber during bioprinting or assembly of the fibers through biotextile methods. We have also demonstrated the ability to control cellular alignment inside the individual fibers (Fig. 4). As mentioned in Sec. II A and indicated in Fig. 2(g), manipulation of flow rates in the microfluidic coaxial device provides the opportunity to change the orientation of internal hydrogel microfilaments. This fact was exploited here to control the internal organization of the cells. Because the encapsulated cells spread along the internal microfilaments, the cellular alignment can be finely tuned by controlling the flow rates. As shown in Fig. 4(a), increasing the ratio of Q_{out}/Q_{in} can deviate the direction of cellular orientation from the fiber axis toward a radial alignment perpendicular to the fiber axis. While a static mixer with both five and six Kenics elements could effectively generate MCHFs with controlled cellular organization, five Kenics elements were used here to generate larger features and better detect and characterize the cellular directionality. The quantitative evaluation of F-actin direction indicates a unidirectional orientation in the angled arrangement [Fig. 4(b)]. The adjustment of cellular orientation with flow rates enables continuous real-time control over the cellular organization within the final scaffold.

C. Cell differentiation in multicompartmental hydrogel fibers: Toward muscle tissue engineering

Fiber-based biofabrication approaches can be employed in production of biomimetic scaffolds for engineering anisotropic tissues such as muscle. Mimicking fibrillar structure of such tissues in bioengineered scaffolds can regulate encapsulated cells' behavior toward enhanced myogenesis.[47–49] Here, as a proof of concept, we have demonstrated the ability of the proposed strategy for supporting myoblast maturation (Fig. 5). The fibers were fabricated using the previously described strategy, with a static mixer having six Kenics elements. A $Q_{out}/Q_{in} = 1$ ratio was applied in the coaxial microfluidic system to ensure the alignment of the microfilaments and therefore the encapsulated cells along the fiber axis. Following fiber fabrication and their subsequent culture for 24 h to allow cellular alignment, the maturation of the myoblast was investigated by evaluating the morphology and gene expression of the cells over time. As indicated in Fig. 5(a), the aligned myoblasts rapidly proliferated, fused, and formed multinucleated myotubes. On day 7 postencapsulation, the hydrogel fiber was completely occupied by highly oriented densely packed myotubes, forming a fascicle-like structure (Fig. S6).

To confirm the results obtained from the morphology analysis, we further evaluated the expression of myogenic markers from the myoblast-laden multicompartmental hydrogel fibers. The transcriptional level of early and late myogenic markers was examined over time using reverse-transcription quantitative polymerase chain reaction (RT-qPCR). In muscle tissue formation, myogenic regulatory factors (MRFs), including myogenic differentiation (MyoD) and MRF4, govern the differentiation of cells toward myofibers.[17,50] Figure 5(b) schematically illustrates the myogenic progression of encapsulated myoblast cells. At the initial differentiation step, aligned myoblasts form myocytes and fuse with each other. These cells then experience secondary fusion, creating myotubes, which can further form muscle fibers. Finally, these myofibers mature to form fascicle-like constructs. In this process, MyoD induces the expression of myogenin, which is necessary for myocyte formation and fusion. In addition, MRF4 plays a dual role, active both in proliferation of undifferentiated myoblasts and as a differentiation gene in cells undergoing maturation. Both myogenin and MRF4 have also been reported to contribute to terminal differentiation.[51,52] Finally, in the matured muscle, sarcomere contractile proteins, such as myosin heavy chain 1 (Myh1), are highly expressed, while MRF4 transcript levels exceed the expression of other MRFs.[17,50] Here, the expression of MyoD in the cell-laden multicompartmental fibers peaked in days 5–7, indicating the differentiation of myoblasts, while the MRF4 level showed a sharp increase on day 7, demonstrating the maturation of the differentiated cells. High levels of myosin heavy chain expression on day 11 further confirm the maturation of cells and formation of fascicle-like structure.

D. Assembly of multicompartmental hydrogel fibers for fabrication of higher-scale constructs

One of the most important advantages of the proposed hydrogel fiber formation is compatibility with existing fiber-based biofabrication

J_ID: APRPG5 DOI: 10.1063/5.0040732 Date: 17-March-21 Stage: Page: 7 Total Pages: 15

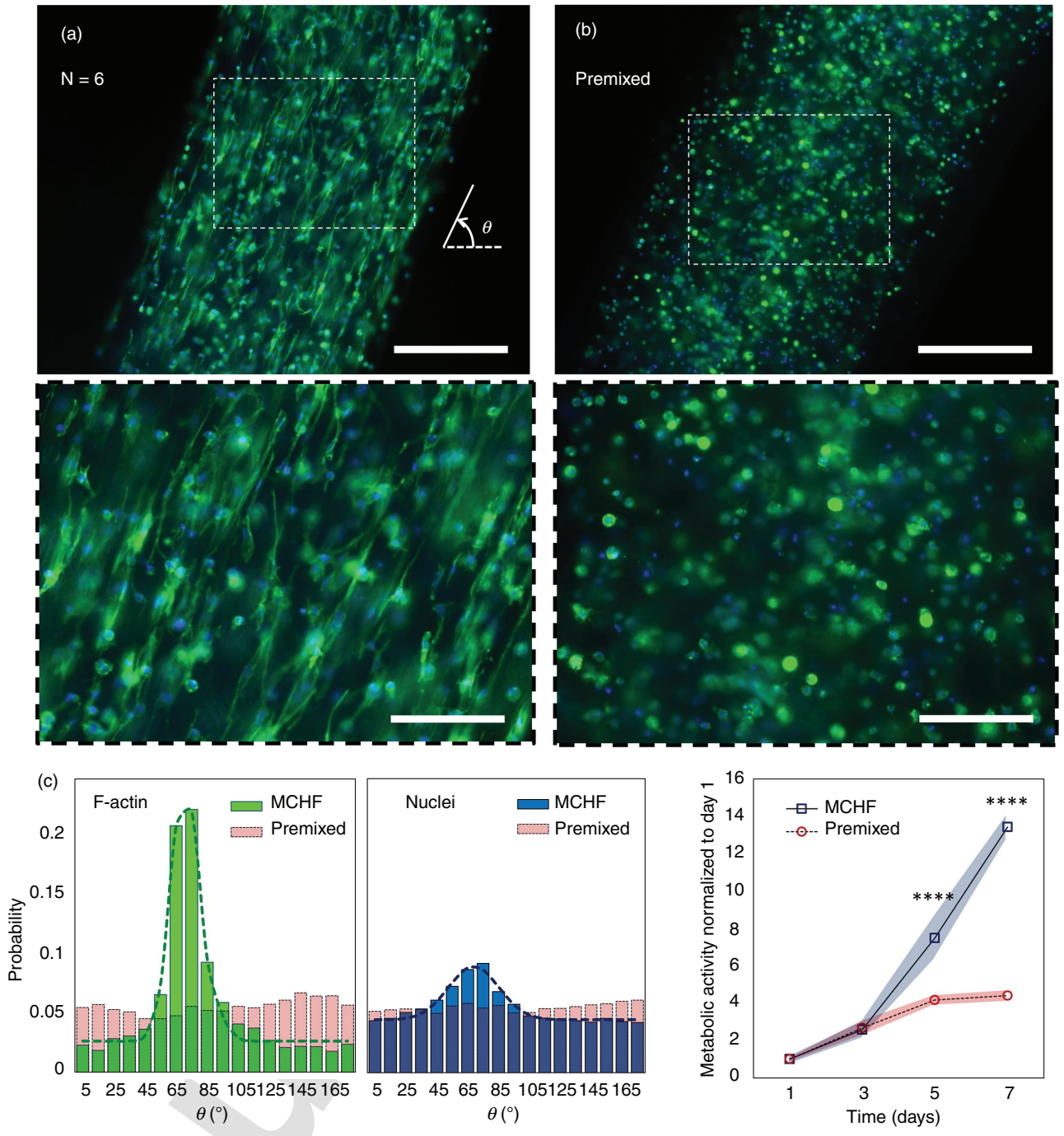

FIG. 3. Cellular organization and metabolic activity in multicompartmental hydrogel fibers. (a) F-actin/DAPI staining demonstrating the alignment of myoblasts along the fiber axis 24 h postencapsulation. A static mixer with six Kenics elements was implemented for fabrication of multicompartmental alginate/GelMA fibers. The bottom image is a magnified representation of the zone indicated by dashed rectangle in the top image. (b) In contrast to the cells cultured in multicompartmental fibers, those cultured in premixed hybrid hydrogel fibers did not demonstrate spreading or alignment. The bottom image is a magnified representation of the zone indicated by the dashed rectangle in the top image. (c) Quantitative evaluation of F-actin cytoskeleton (left) and nuclei (right) directionality within MCHF compared with hydrogel fibers fabricated from premixed bioink. Although the size of the fibers was large compared with the cells' dimension (~50 times), a highly aligned unidirectional organization was observed both in the cytoskeleton and nuclei of the cells cultured in the MCHFs [θ is shown in (a)]. (d) Enhanced metabolic activity of the cells cultured in MCHFs compared with the cells cultured in premixed fibers. n = 4 for each time point. Scale bars are 500 μm for the top row and 200 μm for the bottom magnified images. $^{****}P < 0.0001$.

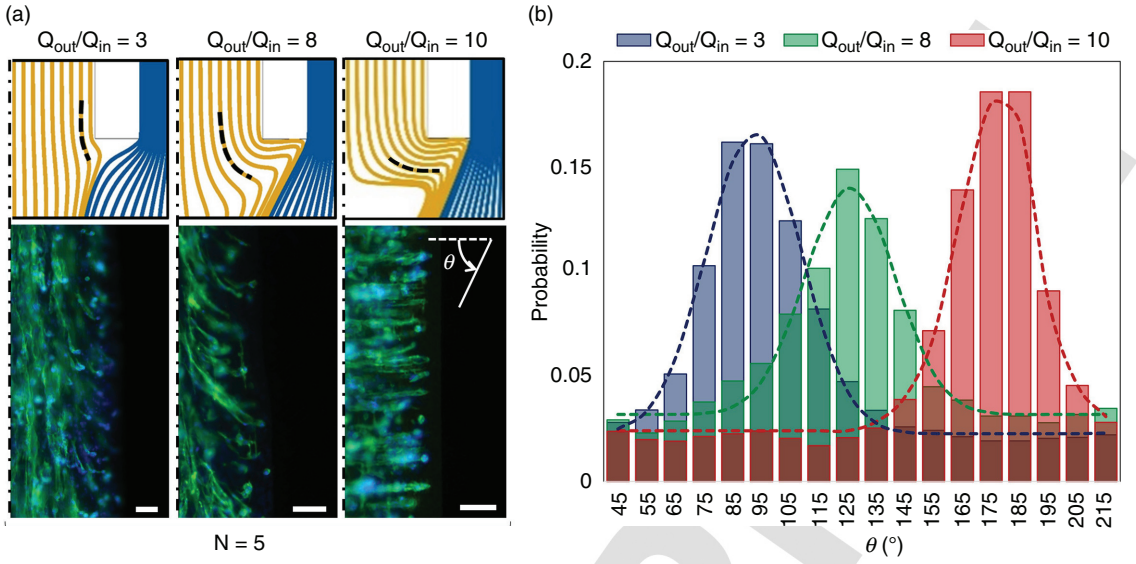

FIG. 4. Real-time control of cellular organization within the multicompartmental fibers. (a) The effect of Q_{out}/Q_{in} ratio on cellular alignment. Increasing the ratio deviates the orientation of the cells in the fibers by deforming the hydrogel flow striations and, therefore, internal microfilament direction. The upper panels show the results of fluid dynamics simulations at the outlet of the microfluidic coaxial channels ($Q_{out}/Q_{in} = 3$, 8, and 10, respectively, from left to right), while the lower panels show the corresponding cellular arrangement demonstrated using F-actin/DAPI staining. Dashed-dotted lines indicate center lines. Scale bars are 500 μm. (b) Distribution of F-actin orientation at different ratios of flow rates, corresponding to the images shown in (a). A static mixer with five Kenics elements was used for formation of internal microfilaments.

methods for constructing higher-scale structures with physiologically relevant dimensions (Fig. 6). Using an extrusion bioprinting device [Fig. S1(b)], fibers were deposited to form a multicompartmental two-layer mesh [Fig. 6(a), (i)] or unidirectional fibrous structures suitable for mimicking anisotropic tissues [Fig. 6(a), (ii)]. A microscopic picture of the printed structure demonstrates that upon printing, the internal microfilaments formed by the static mixer were preserved [Fig. 6(a), (iii)]. The fibers can also be fabricated by wet spinning [Fig. S1(c)] and assembled using various biotextile approaches [Fig. 6(b)]. The multicompartmental fibers were mechanically strong enough to allow easy handling. The mechanical properties of fabricated fibers with different concentrations of alginate and GelMA are shown in Fig. S7. Since the proposed fiber fabrication strategy enables production of relatively large fibers, while preserving the required resolution, the handling challenges would be further reduced. In addition, the large size of the fibers offers minimal assembly steps for production of tissue-scale constructs. Figure 6(c) shows cell-laden assembled constructs fabricated through biotextile processes. The capability for manipulation of the structure of assembled constructs by adjusting the composition, microstructure, and cellular orientation of individual fibers offers a high level of controllability in the biofabrication strategy.

III. DISCUSSION

Controlling cellular organization in biofabrication strategies is one of the most important, but challenging, requirements in engineering of highly organized tissues. This includes biomimetic spatial distribution of the cells as well as specific cellular alignment within the scaffolds. While the spatial distribution of the cells in the scaffolds can be controlled by various top-down or bottom-up biofabrication approaches, controlling the alignment of the cells during biofabrication is still an unmet need. The precise mimicking of cellular organization in biofabrication has the potential not only to regulate encapsulated cells' behavior toward formation of the target tissue but also to promote the functionality of the final maturated tissue. For example, the proper alignment of cells within a muscle enhances the force generation capacity of the tissue.[53] To form such cellular organization, a biofabrication strategy enabling high-resolution control over the microstructure and patterned biomaterials is required. The resolution in the order of cell dimensions can ensure a proper regulation of cellular alignment within the scaffold. To address this demand, a methodology was designed based on two key elements:

1. A robust biofabrication strategy that
   - (i) can form scaffolds with controlled microstructure with feature size in the order of the cell dimension;
   - (ii) is compatible with bioprinting and biotextile assembly methods; and
   - (iii) is simple, low cost, and high throughput.
2. A suitable bioink that
   - (i) supports cell functionality by providing binding sites and biodegradable sequences;
   - (ii) forms stiff microtopographies to direct cellular alignment;
   - (iii) enables rapid cross-linking for compatibility with bioprinting and fiber spinning approaches; and
   - (iv) is mechanically strong enough to form a scaffold with high shape fidelity.

The biofabrication requirements were addressed by development of a method having precise control over the flow of different hydrogel precursors in a microfluidic nozzle. A Kenics static mixer with an optimized number of helical elements was used to divide streams of different hydrogel precursors and create aligned striations of hydrogels with

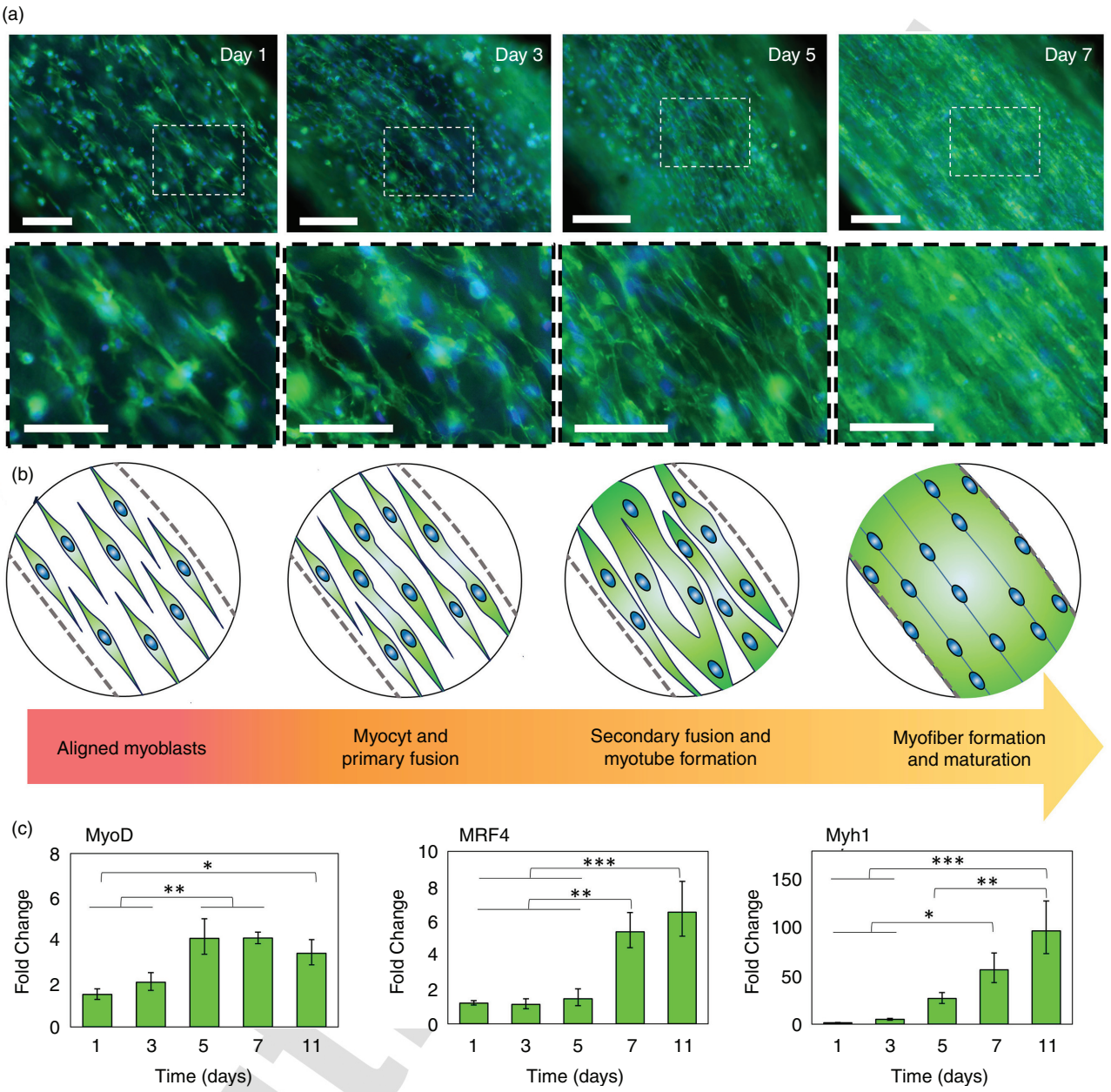

FIG. 5. Application of multicompartmental hydrogel fibers as a promising scaffold for muscle tissue engineering. (a) Morphology analysis of encapsulated myoblasts over a week using F-actin/DAPI staining. As illustrated, highly aligned cells rapidly proliferated, fused with each other, and differentiated toward muscle fiber formation. The bottom row represents the magnified images of the zones indicated in top row by dashed rectangles. Scale bars are 200 μm for the top row and 100 μm for the bottom row. (b) Schematic representation of myoblast myogenesis toward muscle fascicle formation. (c) Myogenic progression of the cells in hydrogel fibers using gene expression analysis with RT-qPCR. The expression of early (MyoD) and late (MRF4 and Myh1) myogenic markers was evaluated over 11 days. Fold change is calculated by normalizing the results to GAPDH as internal reference and day 0 results. n = 3 for each time point. $^{*}P < 0.05$, $^{**}P < 0.01$, $^{***}P < 0.001$.

desired dimensions, comparable to the cell size. Using computational fluid dynamics simulations, we demonstrated that the resolution in this system is not shear or pressure dependent and is improved through the consecutive subdivision of streams without changing the nozzle diameter. This is an important advantage in fluidic systems, specifically microfluidic devices applied in biofabrication of cell-laden constructs. Conventionally, the resolution in extrusion bioprinting is increased with the nozzle diameter. A fine nozzle diameter increases the shear stress applied to the encapsulated cells and significantly decreases their viability.[54] Additionally, the high pressure drop in fine

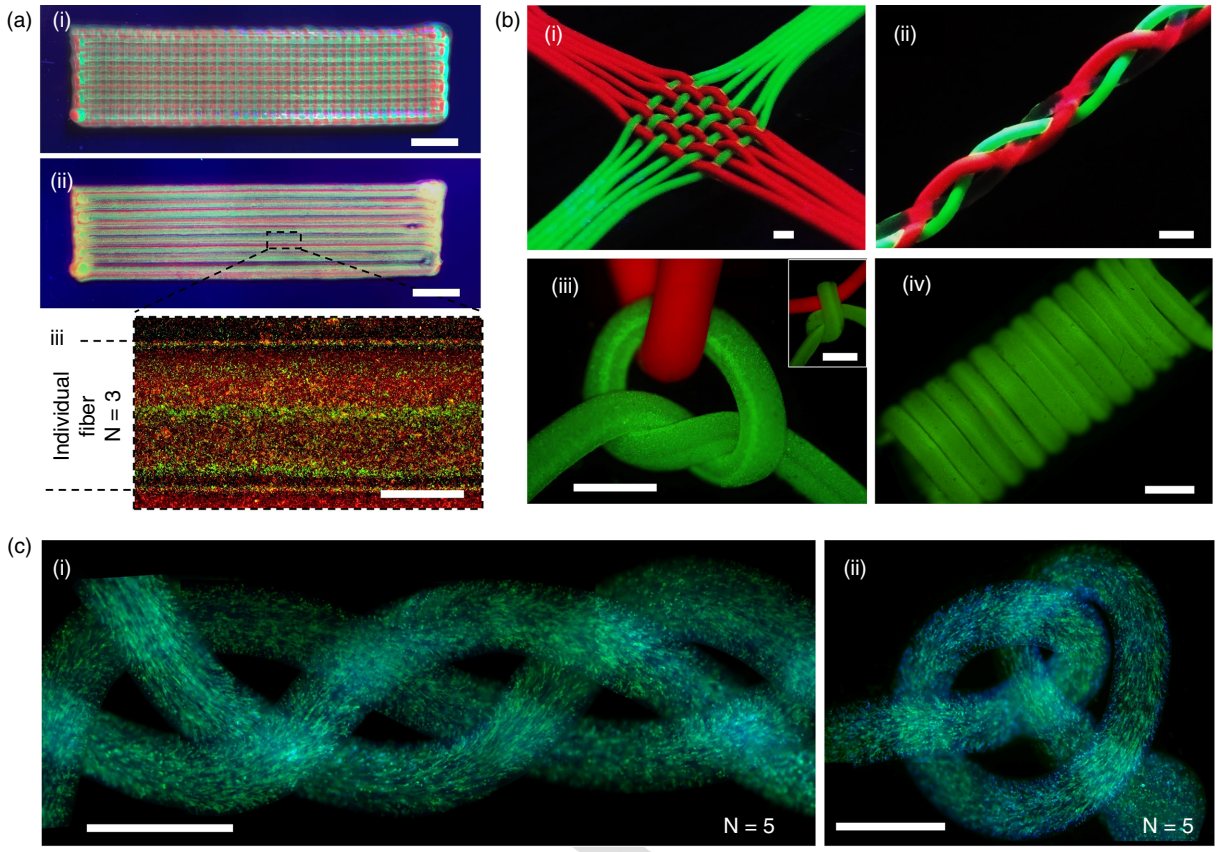

FIG. 6. Application of multicompartmental hydrogel fibers for biofabrication of higher-scale constructs. (a) Bioprinting of multilayered mesh (i) and unidirectional structures (ii). The microscopic picture (iii) confirms preservation of the internal microfilaments generated by a static mixer upon printing. Scale bars are 5 mm for (i) and (ii) and 500 μm for (iii). Three Kenics elements were used for better visibility of different compartments along the fibers. (b) Various biotextile techniques, including weaving (i), braiding (ii), knotting (iii), and coil formation (iv), for biomimetic assembly of multicompartmental hydrogel fibers. The capability for manipulation of the structure of assembled constructs by controlling individual fiber composition is indicated by encapsulation of two different fluorescent particles in the fibers. Scale bars are 2 mm. (c) Cell-laden constructs fabricated through biotextile assembly of multicompartmental hydrogels. F-actin/DAPI assay was used for staining. Scale bars are 2 mm.

AQ7 nozzles, due to energy dissipation by channel wall–mediated hydrodynamic resistance against the fluid flow, necessitates higher extrusion pressure. A higher extrusion pressure can affect the cellular viability and requires the application of pumps with higher power as well as better channel sealing.[54] Finally, a fine nozzle decreases the throughput of the bioprinting, which is of substantial importance in food biomanufacturing.[55] The application of the static mixer in this study resolves these important challenges. Subsequently, a coaxial microfluidic device was implemented to extrude and form hydrogel fibers from the mixture of the hydrogel precursor, controlling the diameter of the fiber and the orientation of internal microfilaments.

Alginate and GelMA were selected to form the components of the bioink in the proposed biofabrication technique. The bioink was designed based on the synergistic interplay of these two materials in which each hydrogel plays crucial roles for addressing the requirements of a suitable bioink. Using the biofabrication method, fibers with internal microstructure consisting of consecutive microfilaments of GelMA and alginate were formed. Within the microstructure, the GelMA filaments provided a cell-permissive environment, while the stiffer, non–cell-permissive alginate sections provided topological and mechanical cues for cell alignment. By controlling the alignment of microfilaments within the hydrogel fiber through manipulation of flow rates in coaxial microchannels, we proposed a real-time control mechanism over the direction of cellular orientation within the individual fibers. This feature enables continuous bioprinting of cell-laden constructs with *in situ*–controlled cellular organization.

We further demonstrated that this biofabrication strategy properly supports cellular activity within the scaffold, in contrast to the hybrid scaffolds fabricated with homogeneously mixed alginate/GelMA hybrid bioink. This is an important outcome since several efforts have been made to harness the printability of the alginate and cell permissibility of the GelMA by application of their hybrid hydrogels, although the internal cell spreading and alignment were limited.[29,36,37] This issue could not be resolved even by introduction of microfilaments inside fiber using a similar static mixer used in this study.[41] This is due to the presence of alginate within the structure, which prevents degradation, and therefore spreading and proliferation, of the encapsulated cells. Here, we demonstrated that

Applied Physics Reviews ARTICLE scitation.org/journal/are

microcompartmentalization in the structure can resolve this problem. Cells can spread and proliferate in the GelMA sections while alginate provides a matrix that allows a printable scaffold with high fidelity.

As a proof of concept, we demonstrated that the multicompartmental hydrogel fibers support cellular maturation toward muscle tissue engineering. The biofabricated hydrogel fibers with internal microfilaments along the fiber axis provide the opportunity for improved mimicking of native muscular tissues and direct myoblast alignment. Staining and gene expression analysis confirmed the high potential of the multicompartmental hydrogel fiber for myogenesis. Fascicle-like constructs with densely packed, highly aligned cellular organization were formed, expressing genes associated with myofiber maturation.

The proposed biofabrication strategy is simple and robust. This system can be easily integrated with any extrusion bioprinting or fiber spinning device to fabricate multicompartmental scaffolds capable of controlling cellular alignment. As a result, we believe that this strategy can provide many opportunities for engineering of highly organized cellular scaffolds.

IV. MATERIALS AND METHODS

A. Materials

Sodium alginate (medium viscosity), $CaCl_2$, type A gelatin from porcine skin, methacrylic anhydride (MA), and 4′,6-diamidino-2-phenylindole (DAPI) were purchased from Sigma-Aldrich. Irgacure 2959 (CIBA Chemicals) was used as photoinitiator (PI). Dulbecco's phosphate buffer saline (DPBS, Gibco), Hank's balanced salt solution (HBSS, Gibco) without calcium and magnesium, Dulbecco's modified eagle medium (DMEM, Gibco), fetal bovine serum (FBS, Gibco), horse serum (Gibco), and penicillin/streptomycin (Gibco) were used for experiments with the cells. Alexa Fluor 488 Phalloidin (Life Technologies) was used for characterization of cells' morphology, while metabolic activity of the cells was examined using PrestoBlue cell viability assay (Invitrogen).

B. Hydrogel preparation

GelMA was prepared according to the well-established protocol,[56] with some modification. Briefly, a 10% solution of gelatin (in DPBS) was prepared by stirring for 1 h at 50 °C. Subsequently, 50 μl MA per 1 g gelatin was added to the mixture slowly and stirred for 3 h at 50 °C and 250 rpm to perform the methacrylation. To stop the reaction, DPBS was added (5:1 ratio of DPBS:GelMA), and dialysis was performed at 40 °C for 5 days using 12–14-kDa molecular weight cut-off tubing (Thermo Fisher Scientific). Finally, the solution was filtered, frozen at −80 °C for 2 days, and lyophilized for 5 days. GelMA precursor was prepared by mixing 2% PI and 10% GelMA solutions in HBSS with a 1:5 volumetric ratio. The alginate precursor was prepared at a 2% concentration in HBSS.

C. Biofabrication of multicompartmental hydrogel fibers

The biofabrication was performed through either bioprinting or wet spinning of multicompartmental hydrogel. In both cases, a static mixer integrated with a coaxial microfluidic device was used as the nozzle [Fig. S1(a)]. The static mixer was prepared by fitting a specific number of 3D-printed Kenics helical elements (66:100:4 ratio of diameter:length:thickness of each element) into a barrel with a conical outlet. The barrel was then sealed with a polydimethylsiloxane plug with two openings for hydrogel injection. The microfluidic device for coaxial flow was fabricated by assembling blunt needles with different gauge sizes (14G and 18G or 19G and 24G). The needles were trimmed to such a size that the tip of the inner needle was located at ∼1 mm from the opening of the outer one. Finally, the microfluidic device was attached to the conical static mixer tip. For experiments with cells, the device was incubated in ethanol (70%) followed by washing with autoclaved distilled water three times.

To accurately adjust the flow rates of hydrogel and $CaCl_2$ solutions, the inlets were connected to syringes using Tygon tubing (Cole-Parmer), and the flows were controlled using syringe pumps (PHD 2000; Harvard Apparatus). Unless otherwise stated, the flow rates of alginate, GelMA, and $CaCl_2$ solutions were set to 1×, 1×, and 2×, in which the × for bioprinting and wet spinning experiments were set to 10 μl/min and 500 μl/min, respectively. In bioprinting experiments, the setup was mounted on the printing head of the bioprinter (Allevi 3). While the flow rates were controlled using separate syringe pumps, the displacement of the nozzle was controlled by the bioprinter [Fig. S1(b)]. For wet spinning [Fig. S1(c)], the nozzle was placed into a $CaCl_2$ bath at 10 °C while the solutions were extruded. A 2% (w/v) $CaCl_2$ solution was used for ionic gelation of alginate followed by 30-s UV cross-linking of the GelMA using a 365 nm/850 mW source placed at a distance of 7 cm from the fibers.

D. Fluid flow characterization and hydrogel fiber topography

Finite element simulations were conducted to evaluate the function of the static mixer and flow-focusing device and to examine the mechanism of highly aligned fibrillar structure formation within the hydrogel fiber. The model was implemented in COMSOL Multiphysics Version 5 using "Laminar Flow" and "Particle Tracing for Fluid Flow" interfaces. First, a 3D model was designed with the dimensions matching the dimensions of the actual static mixer and coaxial microfluidic device. The "Laminar Flow" was then used to simulate the flow of hydrogel and $CaCl_2$ solutions in the channels through solving the Navier-Stokes equations. Different flow rates were applied to the hydrogel and $CaCl_2$ inlets in different simulations, corresponding to the experimental flow rates mentioned in Sec. IV C, while the relative pressure was always set to zero at the outlet. All boundaries were considered to have a "nonslip" condition, and the model was discretized with fine free tetrahedral elements. Finally, the model was solved using "Stationary Solver." To evaluate the pressure inside the channels, the pressure obtained through solving the Navier-Stokes equations (the relative pressure $p = p_{abs} - p_{ref}$, in which p_{abs} is the absolute pressure and p_{ref} is the sea-level pressure) was used. Additionally, the shear stress was calculated postsimulation through multiplication of shear rate (spf.sr) by the fluid viscosity (spf.mu). The maximum pressure P_{max} and the maximum shear stress τ_{max} were determined from the highest values in the simulation domains provided by the software. The maximum pressure generally happens at the channel entrance since it depends on resistance against the flow, while the maximum shear stress usually happens at the fluid/wall interface, where the channel cross-section area is minimum, because it is proportional to the rate of velocity changes. To track the streams of the hydrogels in the static mixer and for the cross-section profile, the

"Particle Tracing for Fluid Flow" interface was used to simulate the movement of 10^4 massless particles in the previously solved velocity field using "Time Dependent Solver." For particle tracing, a "Freeze" boundary condition was set to the channels' walls. To visualize the fiber cross section in the simulations, "Poincaré Map" was implemented, with different colors used for the particles injected from different inlets.

Experimentally, fluorescent particles were used to evaluate the cross-sectional profiles of the fibers. After fabrication, fibers were embedded into 3% agarose gel and sliced using a surgical blade. To evaluate the formation of GelMA microfilaments in the alginate matrix, phase contrast microscopy was performed on a Zeiss Observer D1 microscope. The diameter of final fibers was measured using ZEN 2 software.

E. Cell culture

Murine myoblast cell line C2C12 (ATCC) was cultured in DMEM supplemented with 10% [volume/volume (v/v)] FBS and 1% (v/v) penicillin/streptomycin (culture medium). Cells were incubated at 37 °C in a humidified 5% CO_2 atmosphere and subcultured at 80%–90% confluence. Cell passages 6–8 were utilized for experiments.

For the encapsulation of C2C12 myoblasts, cells were trypsinized and detached followed by resuspension in culture medium with the density of 20×10^6 cells/ml. The solution was then added to GelMA precursor with the volumetric ratio of 1:20 and mixed. Subsequently, cell-laden multicompartmental hydrogel fibers were formed as previously described. After fabrication, the fibers were incubated in the culture medium for future analysis. For evaluating maturation of the myoblasts in the scaffolds, culture medium was replaced with differentiation medium 2 days after biofabrication. The differentiation medium, which was prepared using DMEM supplemented with 2% (v/v) horse serum and 1% (v/v) penicillin/streptomycin, was replaced every 48 h.

F. Cellular morphology characterization

F-actin/DAPI staining was employed for characterization of cells' morphology. The staining was conducted at room temperature, and HBSS was used for washing steps and solution preparation. Samples were fixed using 4% paraformaldehyde (Electron Microscopy Sciences) for 30 min, washed three times, and stained using phalloidin and DAPI as described in the manufacturer's manual, with small modifications. Briefly, cells were permeabilized using 0.2% (v/v) Triton X-100 (Sigma) for 10 min, washed three times, and followed by blocking with 1% (w/v) bovine serum albumin (Sigma). The samples were then incubated for 40 min in phalloidin (1.65 μM), protected from the light, and subsequently washed three times. Nuclei of the cells were then stained using DAPI solution (5 μg/ml) for 15 min, and finally, the samples were washed three times. Fluorescence microscopy was performed on the Zeiss Observer D1 microscope employing an X-Cite 120Q fluorescence source. Subsequently, quantitative analysis of the cellular orientation was performed using Directionality or OrientationJ plugins of FIJI open-source software.[57]

G. Determination of metabolic activity

Metabolic activity of the encapsulated myoblasts within the hydrogel fiber constructs was measured using a PrestoBlue viability assay. For this purpose, the fabricated hydrogel fibers were cut into smaller segments (~1 cm) and incubated with 10% PrestoBlue solution (v/v in culture medium) at 37 °C. After 1 h, the solution was collected in a 96-well plate, and its fluorescent intensity (550 ex/600 em) was measured using a plate reader (Synergy 2; BioTek). The evaluation was performed 1, 3, 5, and 7 days after fiber fabrication. The background intensity (corresponding to wells with 10% PrestoBlue solution, excluding cell-laden fibers) was subtracted, and the results were normalized with respect to the values of day 1.

H. Reverse-transcription quantitative polymerase chain reaction

Expression levels of three myoblast differentiation genes (MyoD, MRF4, and Myh1) were evaluated using RT-qPCR after 0, 1, 3, 5, 7, and 11 days of fiber fabrication. Total RNA was extracted using RNeasy Plus Mini Kit (QIAGEN), and 1 μg of extracted RNA was reverse-transcribed using QuantiTect Reverse Transcription Kit (QIAGEN) according to the manufacturer's protocols. Real-time PCR was performed on a Rotor-Gene Q (QIAGEN) using 2 μl cDNA template, 2 μl primer set, and 16 μl SYBR Green Master Mix (Fermentas). Thermal cycle conditions were 10 min denaturation at 95 °C followed by 45 cycles of 10 s at 95 °C, 30 s at 60 °C, and 30 s at 72 °C. The results were normalized to that of GAPDH as reference housekeeping gene and then to the results of day 0 using $2^{-\Delta\Delta Ct}$ method. The primer sequences used for amplification are listed in Table S1.

I. Statistical analysis

All experiments were performed at least in triplicate, and the results were presented as average ± standard deviation. Comparison between the groups was performed through one- or two-way analysis of variance, and results were presented as $^{*}P < 0.05$, $^{**}P < 0.01$, $^{***}P < 0.001$, and $^{****}P < 0.0001$ in which P is the adjusted P value.

AUTHORS' CONTRIBUTIONS

M.S. and A.T. conceived and designed the research. M.S. and F.A. performed the experiments. M.S., K.M.-A., and A.T. analyzed the results. M.S., K.M.-A., M.M.A., G.T.-d.S., and A.T. participated in writing the manuscript. All authors contributed to revising and editing the manuscript.

SUPPLEMENTARY MATERIAL

See the supplementary material for additional information on the applied devices, further characterization of the bioprinted MCHFs, and primer design for gene expression analysis.

ACKNOWLEDGMENTS

Financial support from the National Institutes of Health (Grant Nos. GM126831, and AR073822) is gratefully acknowledged. M.M.A. and G.T.-d.S. acknowledge funding provided from CONACyT (Consejo Nacional de Ciencia y Tecnología, Mexico). G.T.-d.S. acknowledges funding received from L'Oréal-UNESCO-CONACyT-AMC (National Fellowship for Women in Science, Mexico).

DATA AVAILABILITY

The data that support the findings of this study are available within the article and its supplementary material. Additional data that

support the findings of this study are available from the corresponding author upon reasonable request.

REFERENCES

[1]S. M. Naseer, A. Manbachi, M. Samandari, P. Walch, Y. Gao, Y. S. Zhang, F. Davoudi, W. Wang, K. Abrinia, and J. M. Cooper, Biofabrication **9**(1), 015020 (2017).

[2]G. Trujillo-de Santiago, M. M. Alvarez, M. Samandari, G. Prakash, G. Chandrabhatla, P. I. Rellstab-Sánchez, B. Byambaa, P. Pour Shahid Saeed Abadi, S. Mandla, R. K. Avery, A. Vallejo-Arroyo, A. Nasajpour, N. Annabi, Y. S. Zhang, and A. Khademhosseini, Mater. Horiz. **5**(5), 813–822 (2018).

[3]T. Turiv, J. Krieger, G. Babakhanova, H. Yu, S. V. Shiyanovskii, Q.-H. Wei, M.-H. Kim, and O. D. Lavrentovich, Sci. Adv. **6**(20), eaaz6485 (2020).

[4]S. Zhang, X. Liu, S. F. Barreto-Ortiz, Y. Yu, B. P. Ginn, N. A. DeSantis, D. L. Hutton, W. L. Grayson, F.-Z. Cui, B. A. Korgel, S. Gerecht, and H.-Q. Mao, Biomaterials **35**(10), 3243–3251 (2014).

[5]M. Mirbagheri, V. Adibnia, B. R. Hughes, S. D. Waldman, X. Banquy, and D. K. Hwang, Mater. Horiz. **6**(1), 45–71 (2019).

[6]T. E. Brown and K. S. Anseth, Chem. Soc. Rev. **46**(21), 6532–6552 (2017).

[7]M. Nikkhah, J. S. Strobl, R. De Vita, and M. Agah, Biomaterials **31**(16), 4552–4561 (2010).

[8]G. Huang, F. Li, X. Zhao, Y. Ma, Y. Li, M. Lin, G. Jin, T. J. Lu, G. M. Genin, and F. Xu, Chem. Rev. **117**(20), 12764–12850 (2017).

[9]J. Leijten, J. Seo, K. Yue, G. Trujillo-de Santiago, A. Tamayol, G. U. Ruiz-Esparza, S. R. Shin, R. Sharifi, I. Noshadi, M. M. Álvarez, Y. S. Zhang, and A. Khademhosseini, Mater. Sci. Eng.: R: Rep. **119**, 1–35 (2017).

[10]Y. Luo and M. S. Shoichet, Nat. Mater. **3**(4), 249–253 (2004).

[11]S.-H. Lee, J. J. Moon, and J. L. West, Biomaterials **29**(20), 2962–2968 (2008).

[12]H. Aubin, J. W. Nichol, C. B. Hutson, H. Bae, A. L. Sieminski, D. M. Cropek, P. Akhyari, and A. Khademhosseini, Biomaterials **31**(27), 6941–6951 (2010).

[13]M. Zhu, W. Li, X. Dong, X. Yuan, A. C. Midgley, H. Chang, Y. Wang, H. Wang, K. Wang, P. X. Ma, H. Wang, and D. Kong, Nat. Commun. **10**(1), 4620 (2019).

[14]M. Nikkhah, N. Eshak, P. Zorlutuna, N. Annabi, M. Castello, K. Kim, A. Dolatshahi-Pirouz, F. Edalat, H. Bae, Y. Yang, and A. Khademhosseini, Biomaterials **33**(35), 9009–9018 (2012).

[15]P. Heher, B. Maleiner, J. Prüller, A. H. Teuschl, J. Kollmitzer, X. Monforte, S. Wolbank, H. Redl, D. Rünzler, and C. Fuchs, Acta Biomater. **24**, 251–265 (2015).

[16]T. Matsumoto, J.-I. Sasaki, E. Alsberg, H. Egusa, H. Yatani, and T. Sohmura, PloS One **2**(11), e1211 (2007).

[17]S. Ahadian, J. Ramón-Azcón, S. Ostrovidov, G. Camci-Unal, V. Hosseini, H. Kaji, K. Ino, H. Shiku, A. Khademhosseini, and T. Matsue, Lab on a Chip **12**(18), 3491–3503 (2012).

[18]K. Donnelly, A. Khodabukus, A. Philp, L. Deldicque, R. G. Dennis, and K. Baar, Tissue Eng. Part C Methods **16**(4), 711–718 (2010).

[19]S. Ostrovidov, V. Hosseini, S. Ahadian, T. Fujie, S. P. Parthiban, M. Ramalingam, H. Bae, H. Kaji, and A. Khademhosseini, Tissue Eng. Part B Rev. **20**(5), 403–436 (2014).

[20]S. Ostrovidov, S. Salehi, M. Costantini, K. Suthiwanich, M. Ebrahimi, R. B. Sadeghian, T. Fujie, X. Shi, S. Cannata, and C. Gargioli, Small **15**(24), 1805530 (2019).

[21]S. Jana, S. K. L. Levengood, and M. Zhang, Adv. Mater. **28**(48), 10588–10612 (2016).

[22]D. Neal, M. S. Sakar, L.-L. S. Ong, and H. H. Asada, Lab on a Chip **14**(11), 1907–1916 (2014).

[23]R. D. Pedde, B. Mirani, A. Navaei, T. Styan, S. Wong, M. Mehrali, A. Thakur, N. K. Mohtaram, A. Bayati, and A. Dolatshahi-Pirouz, Adv. Mater. **29**(19), 1606061 (2017).

[24]A. Tamayol, M. Akbari, N. Annabi, A. Paul, A. Khademhosseini, and D. Juncker, Biotechnol. Adv. **31**(5), 669–687 (2013).

[25]M. Costantini, S. Testa, P. Mozetic, A. Barbetta, C. Fuoco, E. Fornetti, F. Tamiro, S. Bernardini, J. Jaroszewicz, and W. Święszkowski, Biomaterials **131**, 98–110 (2017).

[26]T. K. Merceron, M. Burt, Y.-J. Seol, H.-W. Kang, S. J. Lee, J. J. Yoo, and A. Atala, Biofabrication **7**(3), 035003 (2015).

[27]H.-W. Kang, S. J. Lee, I. K. Ko, C. Kengla, J. J. Yoo, and A. Atala, Nat. Biotechnol. **34**(3), 312 (2016).

[28]H. Onoe, T. Okitsu, A. Itou, M. Kato-Negishi, R. Gojo, D. Kiriya, K. Sato, S. Miura, S. Iwanaga, and K. Kuribayashi-Shigetomi, Nat. Mater. **12**(6), 584 (2013).

[29]A. Tamayol, A. H. Najafabadi, B. Aliakbarian, E. Arab-Tehrany, M. Akbari, N. Annabi, D. Juncker, and A. Khademhosseini, Adv. Healthcare Mater. **4**(14), 2146–2153 (2015).

[30]S. Zhang, X. Liu, S. F. Barreto-Ortiz, Y. Yu, B. P. Ginn, N. A. DeSantis, D. L. Hutton, W. L. Grayson, F.-Z. Cui, and B. A. Korgel, Biomaterials **35**(10), 3243–3251 (2014).

[31]A. Fallahi, I. K. Yazdi, L. Serex, E. Lesha, N. Faramarzi, F. Tarlan, H. Avci, R. Costa-Almeida, F. Sharifi, C. Rinoldi, M. E. Gomes, S. R. Shin, A. Khademhosseini, M. Akbari, and A. Tamayol, ACS Biomater. Sci. Eng. **6**(2), 1112–1123 (2020).

[32]W. Liu, Z. Zhong, N. Hu, Y. Zhou, L. Maggio, A. K. Miri, A. Fragasso, X. Jin, A. Khademhosseini, and Y. S. Zhang, Biofabrication **10**(2), 024102 (2018).

[33]K. Yue, G. Trujillo-de Santiago, M. M. Alvarez, A. Tamayol, N. Annabi, and A. Khademhosseini, Biomaterials **73**, 254–271 (2015).

[34]B. J. Klotz, D. Gawlitta, A. J. W. P. Rosenberg, J. Malda, and F. P. W. Melchels, Trends Biotechnol. **34**(5), 394–407 (2016).

[35]G. Ying, N. Jiang, C. Yu, and Y. S. Zhang, Bio-Des. Manuf. **1**(4), 215–224 (2018).

[36]C. Colosi, S. R. Shin, V. Manoharan, S. Massa, M. Costantini, A. Barbetta, M. R. Dokmeci, M. Dentini, and A. Khademhosseini, Adv. Mater. **28**(4), 677–684 (2016).

[37]K. Zhu, N. Chen, X. Liu, X. Mu, W. Zhang, C. Wang, and Y. S. Zhang, Macromolecular Bioscience **18**(9), 1800127 (2018).

[38]K. Y. Lee and D. J. Mooney, Prog. Polym. Sci. **37**(1), 106–126 (2012).

[39]A. K. Miri, I. Mirzaee, S. Hassan, S. M. Oskui, D. Nieto, A. Khademhosseini, and Y. S. Zhang, Lab on a Chip **19**(11), 2019–2037 (2019).

[40]D. M. Hobbs and F. J. Muzzio, Chem. Eng. J. **67**(3), 153–166 (1997).

[41]C. Chávez-Madero, M. D. de Leon-Derby, M. Samandari, C. F. Ceballos-González, E. J. Bolívar-Monsalve, C. C. Mendoza-Buenrostro, S. Holmberg, N. A. Garza-Flores, M. A. Almajhadi, and I. González-Gamboa, Biofabrication **12**, 035023 (2020).

[42]M. Samandari, F. Alipanah, S. Haghjooy Javanmard, and A. Sanati-Nezhad, Sens. Actuators B Chem. **291**, 418–425 (2019).

[43]W. Bian, B. Liau, N. Badie, and N. Bursac, Nat. Protoc. **4**(10), 1522 (2009).

[44]W. Bian and N. Bursac, Biomaterials **30**(7), 1401–1412 (2009).

[45]G. Agrawal, A. Aung, and S. Varghese, Lab on a Chip **17**(20), 3447–3461 (2017).

[46]H. Liu, M. Wu, Y. Jia, L. Niu, G. Huang, and F. Xu, NPG Asia Mater. **12**(1), 45 (2020).

[47]V. Hosseini, S. Ahadian, S. Ostrovidov, G. Camci-Unal, S. Chen, H. Kaji, M. Ramalingam, and A. Khademhosseini, Tissue Eng. Part A **18**(23–24), 2453–2465 (2012).

[48]P. Bajaj, B. Reddy, L. Millet, C. Wei, P. Zorlutuna, G. Bao, and R. Bashir, Integr. Biol. **3**(9), 897–909 (2011).

[49]P. Y. Wang, H. T. Yu, and W. B. Tsai, Biotechnol. Bioengineering **106**(2), 285–294 (2010).

[50]P. S. Zammit, Semin Cell Dev. Biol. **72**, 19–32 (2017).

[51]Y. X. Wang and M. A. Rudnicki, Nat. Rev. Mol. Cell Biol. **13**(2), 127 (2012).

[52]T. Braun and M. Gautel, Nat. Rev. Mol. Cell Biol. **12**(6), 349 (2011).

[53]S. H. Lim and H.-Q. Mao, Adv. Drug Deliv. Rev. **61**(12), 1084–1096 (2009).

[54]S. V. Murphy and A. Atala, Nat. Biotechnol. **32**(8), 773–785 (2014).

[55]Z. F. Bhat, S. Kumar, and H. Fayaz, J. Integr. Agriculture **14**(2), 241–248 (2015).

[56]J. W. Nichol, S. T. Koshy, H. Bae, C. M. Hwang, S. Yamanlar, and A. Khademhosseini, Biomaterials **31**(21), 5536–5544 (2010).

[57]J. Schindelin, I. Arganda-Carreras, E. Frise, V. Kaynig, M. Longair, T. Pietzsch, S. Preibisch, C. Rueden, S. Saalfeld, B. Schmid, J.-Y. Tinevez, D. J. White, V. Hartenstein, K. Eliceiri, P. Tomancak, and A. Cardona, Nat. Meth. **9**(7), 676–682 (2012).